Proceedings of the International Symposium on Physics of Materials (ISPMA13)

Anisotropic Elastic and Acoustic Properties of Bulk Graphene Nanoplatelets Consolidated by Spark Plasma Sintering

M. Koller[a], H. Seiner[b,*], M. Landa[b], A. Nieto[c] and A. Agarwal[c]

[a]Faculty of Nuclear Sciences and Physical Engineering, Czech Technical University in Prague, Trojanova 13, 120 00 Prague 2, Czech Republic

[b]Institute of Thermomechanics, Academy of Sciences of the Czech Republic, Dolejškova 5, 182 00 Prague 8, Czech Republic

[c]Department of Mechanical and Materials Engineering, Florida International University, 10555 West Flagler Str., EC 3464, Miami, FL 33174, USA

Elastic anisotropy and acoustic attenuation in bulk material consisting of consolidated graphene nanoplatelets are studied. The material was prepared by spark plasma sintering, and exhibits highly anisotropic microstructure with the graphene nanoplatelets oriented perpendicular to the spark plasma sintering compression axis. The complete tensor of elastic constants is obtained using a combination of two ultrasonic methods: the through-transmission method and the resonant ultrasound spectroscopy. It is shown that the examined material exhibits very strong anisotropy both in the elasticity (the Young moduli in directions parallel to the graphene nanoplatelets and perpendicular to them differ by more than 20 times) and in the attenuation, where the dissipative effect of the internal friction in the graphene nanoplatelets combines with strong scattering losses due to the porosity. The results are compared with those obtained for ceramic-matrix/graphene nanoplatelet composites by the same ultrasonic methods.

DOI: 10.12693/APhysPolA.128.670

PACS: 43.35.Cg, 81.40.Jj, 81.05.ue, 81.20.Ev

1. Introduction

Graphene exhibits unique mechanical properties, such as superior tensile strength [1] and extremely high in-plane elastic modulus [2]. In order to utilize these properties for enhancement of the mechanical performance of ceramics, graphene nanoparticles (such as nanotubes and nanoplatelets) are often used as fillers for ceramic matrix composites (CMCs) [3–5]. Various CMCs with highly oriented graphene-based filaments were prepared by the spark plasma sintering (SPS) technique [6–8]. These composite materials exhibit, besides the expected improved fracture toughness, also significant anisotropies in electric conductivity [6], thermal conductivity [7, 9], elastic stiffness and internal friction [10]. Recently, Nieto et al. [11] reported on a bulk material consisting purely of the graphene nanoplatelets (GNPs) consolidated together by the SPS. This material was shown to exhibit unique tribological properties, utilizing the lubricating effect of graphene. However, the highly porous anisotropic microstructure of this material can be expected also to induce extremely strong anisotropy of elastic and acoustic properties. Such an analysis is carried out in this paper, with the main aim to show the relation between the orientation of the GNPs and the macroscopic elasticity and elastodynamics of the bulk material.

*corresponding author; e-mail: hseiner@it.cas.cz

2. Material and samples

The examined material was a bulk aggregate of GNPs consolidated by SPS. A detailed description of the synthesis and properties of this material can be found elsewhere [11], here we bring only a brief summary: GNPs (XG Sciences, US) with thickness of 6 to 8 nm (≈20 layers of graphene) and average diameter of 15 μm were consolidated by SPS at 1850 °C with pressure 80 MPa for holding time of 10 min. The obtained bulk pellet had the thickness of 3 mm and diameter of 20 mm. The mass density of bulk GNPs was measured as 2.11 g/cm^3 which is significantly higher than the density 1.82 g/cm^3 of the original GNP powder.

After SPS consolidation, GNPs were uniformly oriented with their preferred plane perpendicular to the thickness of the sample, as seen in Fig. 1. The Raman spectroscopy (see [11] for more details) proved that individual GNPs retained their graphene content after SPS consolidation and did not transform to any other allotrope of carbon. Some of the individual GNPs were not strictly straight, but they were bent and folded at some places resulting from high applied pressure during SPS processing.

At the macroscale, the material shown in Fig. 1 can be expected to exhibit transversal isotropy, i.e. rotational symmetry about the SPS compression axis, as usual for SPSed composites with spatially anisotropic arrangement of the individual constituents [10].

The anisotropic elasticity of such a material is describable by five independent elastic coefficients: c_{11}, c_{12}, c_{13},

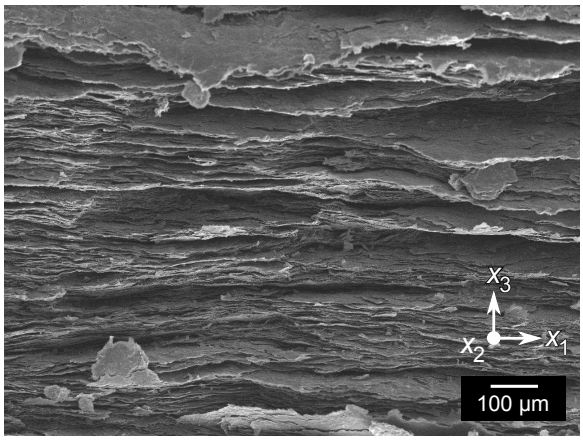

Fig. 1. Scanning electron micrograph of a fracture surface of the examined material. The vertical axis is parallel to the SPS pressing direction, the layered structure outlines the orientation of the GNPs.

c_{33} and c_{44} for the coordinate system oriented such that the axis x_3 is perpendicular to the GNPs. However, in this case it is more illustrative to use $c_{66} = (c_{11} - c_{12})/2$ as one of the independent coefficient instead of c_{12}, as c_{66} represents the shear modulus for shearing perpendicular to the platelets, and can be, thus, directly compared to the shear modulus along the platelets c_{44}.

From the SPS pellet, samples for the ultrasonic characterization were cut out. Two sets of rectangular parallelepiped-like samples were prepared: The first set (4 samples) had the largest faces of the samples parallel to preferred orientation of the GNPs and varying thicknesses (0.52, 0.82, 0.88 and 1.07 mm) in direction perpendicular to this largest face. The second set (3 samples, thicknesses 0.72, 0.88 and 1.25 mm) had the largest faces perpendicular to the GNPs preferred plane. These samples were used for the through-transmission method measurements [12]. Hereafter, the samples from these two sets will be denoted as $T^{\parallel}_{1-4}$ and $T^{\perp}_{1-3}$, respectively, where the symbol in the superscript denotes the orientation of the sample with respect to the GNPs and the number in the subscript is the number of the sample. Additionally, two samples in forms of thin rectangular plates were prepared for the resonant ultrasound spectroscopy (RUS, [13, 14]) measurements. One of these plates (thickness 0.21 mm, lateral dimensions 2.27 mm ×3.40 mm) was oriented parallel to the preferential orientation of the GNPs, the second one (thickness 0.40 mm, lateral dimensions 1.87 mm ×2.81 mm) was oriented perpendicularly to this plane. These samples will be denoted as RUS$^{\parallel}$ and RUS$^{\perp}$, respectively.

3. Experimental

Two ultrasonic methods were applied to the prepared samples. Firstly, the velocities of longitudinal and transverse elastic waves traveling in directions perpendicular and parallel to the GNPs, were obtained by through-transmission measurements on sets $T^{\parallel}_{1-4}$ and $T^{\perp}_{1-3}$. For the set $T^{\perp}_{1-3}$ (i.e. for the propagation along the GNPs) shear waves polarized both along the GNPs and perpendicular to them were detected; for the set $T^{\parallel}_{1-4}$ (i.e. propagation in direction perpendicular to GNPs), no such distinguishing between the polarization directions was necessary, since all possible polarization directions of the shear waves propagation along the x_3 axis are equivalent due to the transversal isotropy.

Then, the vibrational spectra of free elastic vibrations of samples RUS$^{\parallel}$ and RUS$^{\perp}$ were recorded using the contact-less RUS setup described in details in [14]. As shown for example in [15], the through-transmission method and the RUS are complementary to each other, since the through-transmission method is highly sensitive to the hard (mostly longitudinal) elastic coefficients, while the RUS measurements are suitable mainly for the determination of the softest (mostly shear) elastic coefficients.

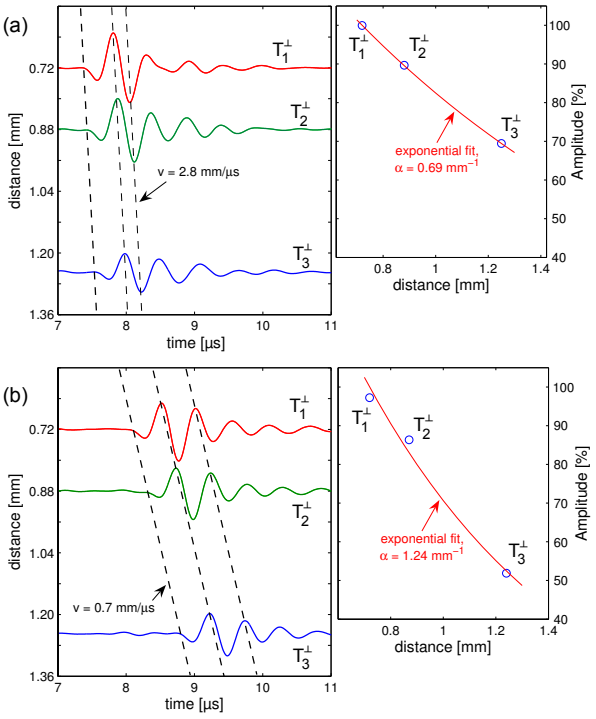

Fig. 2. Experimental data processing examples for transmission through measurements on the samples belonging to the set $T^{\perp}_{1-3}$: (a) shear waves polarized along the GNPs; (b) shear waves polarized parallel to the GNPs.

For the through-transmission measurements, ultrasonic transducers with various nominal frequencies were used, in order to analyze the possible frequency dependence. For the longitudinal wave measurements, transducers at 5 MHz and 10 MHz were used, and for the shear (transversal) measurements, transducers at 2 MHz

and 5 MHz were used. In addition to the velocities of the acoustic waves, the through-transmission measurements enabled also the determination of the acoustic attenuation coefficients α for the individual propagation modes. For each set of the samples, this coefficient was determined from the amplitudes A of the transmitted signals by assuming [12]:

$$A = A_0 \exp(-\alpha d) \quad (1)$$

where A_0 is a constant and d is the traveling distance. Figure 2 shows an example of through-transmission measurement results for determination of the velocity (from the times-of-flight of the waves through the samples) and of the attenuation coefficient (from the amplitudes; the experimental error in α was then determined from the goodness-of-fit of the $A(d)$ data by relation (1)).

The RUS spectra for the samples were recorded in the frequency range 50–500 kHz. Due to the high damping, only a very limited number of resonant peaks was detectable for each sample. In particular, for sample RUS$^{\perp}$, 7 resonant peaks were detected, and for sample RUS$^{\parallel}$, 8 resonant peaks were detected. For each detected resonant peak, also the corresponding modal shape of vibrations was determined by a scanning laser vibrometer.

TABLE I

Results of longitudinal wave through-transmission measurements: velocities v and attenuation coefficients α.

Frequency	Direction	v [mm/μs]	α [mm^{-1}]
5 MHz	$\parallel$ GNPs	5.6±0.1	0.9±0.3
10 MHz	$\parallel$ GNPs	4.7±0.2	1.4±0.3
5 MHz	$\perp$ GNPs	1.3±0.1	2.9±0.7
10 MHz	$\perp$ GNPs	1.2±0.1	5.2±1.0

TABLE II

Results of shear wave through-transmission measurements: velocities v and attenuation coefficients α for different polarization orientations.

Freq.	Direct.	Polariz.	v [mm/μs]	α[mm^{-1}]
2 MHz	$\perp$ GNPs	$\parallel$ GNPs	0.68±0.03	2.1±0.5
5 MHz	$\perp$ GNPs	$\parallel$ GNPs	0.68±0.02	2.0±0.5
2 MHz	$\parallel$ GNPs	$\perp$ GNPs	0.73±0.03	0.7±0.2
5 MHz	$\parallel$ GNPs	$\perp$ GNPs	0.77±0.03	1.1±0.3
2 MHz	$\parallel$ GNPs	$\parallel$ GNPs	2.8±0.2	1.2±0.5
5 MHz	$\parallel$ GNPs	$\parallel$ GNPs	2.9±0.2	1.3±0.5

4. Results and discussion

The results of the through-transmission method (the velocities of the propagation and the corresponding attenuation coefficients) for both sets of samples are listed in Tables I and II. It is clearly seen that the velocity of both the longitudinal and the shear waves exhibits strong anisotropy, and so does the attenuation coefficient. Systematically, the velocities of propagation for all modes and at all frequencies in directions along the GNPs are significantly higher than the corresponding velocities in directions perpendicular to the GNPs.

Only the longitudinal waves appear to be frequency-dependent; especially the velocity of propagation along the GNPs and the corresponding attenuation coefficient differ significantly for 10 MHz and for 5 MHz. This indicates that there is some wave-guiding effect of the platelets occurring in the material.

Another interesting phenomenon appears for the shear waves. From assuming the transversal isotropy, the velocity of the shear waves propagating along the x_3 direction (and polarized along the x_1x_2 plane) should be exactly the same as the velocity of the shear waves propagating along the x_1 direction and polarized along the x_3 direction. Similar equality should be valid also between the attenuation coefficients, providing that the viscoelasticity of the material exhibits the same symmetry class as the elasticity. However, as seen in Table II, the waves propagating perpendicularly to GNPs (i.e. along the x_3 direction) and polarized along them are significantly slower and more attenuated than those propagating along GNPs and polarized perpendicular to them. This discrepancy can be easily explained by the fact that the attenuation of the waves propagation perpendicular to the GNPs is given not only by the viscoelasticity of the material but also by scattering of the waves on flat pores and imperfect bondings between the platelets. This scattering effectively increases the attenuation and decreases the measured velocity of propagation [16]. The observed large difference in both the velocities and the attenuation coefficients indicates that the effect of scattering is very strong; such pronounced anisotropic scattering is expectable with respect to the layered structure of the material.

The outputs of the both experimental methods (i.e. the velocities of longitudinal and shear waves in the given directions and the resonant frequencies of the RUS samples) were recalculated into the elastic coefficients by using a joint inverse procedure described in [17]. This procedure finds such a set of elastic constants that the misfit between the input parameters (i.e. the experimentally obtained velocities and the resonant frequencies) and the values of these parameters calculated for the this set of elastic constants is minimal in the least squares sense. For this procedure, the velocity data obtained at lower frequencies (5 MHz for the longitudinal waves and 2 MHz for the shear waves) were used.

The resulting elastic constants were $c_{11} = (66.17 \pm 2.34)$ GPa, $c_{13} = (9.14 \pm 1.29)$ GPa, $c_{33} = (3.57 \pm 0.51)$ GPa, $c_{44} = (1.15 \pm 0.05)$ GPa, and $c_{66} = (17.76 \pm 1.71)$ GPa, where the errors were calculated by a sensitivity analysis described in [14]. This set of elastic constants confirms the strong anisotropy deduced from the through-transmission measurements: the longitudinal stiffness along the platelets (c_{11}) is significantly stiffer than perpendicular to them (c_{33}); similar difference can be seen between the shear stiffness along the platelets (c_{44}) and perpendicular to them (c_{66}). In Fig. 3, these

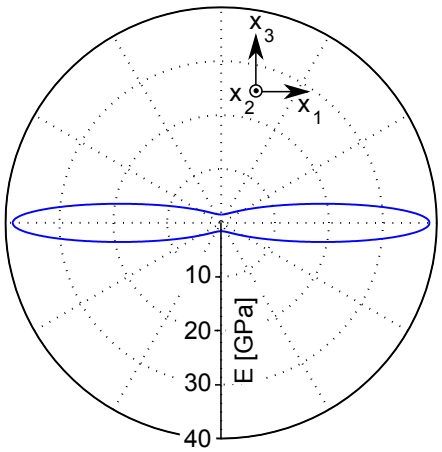

Fig. 3. Directional dependence of the Young modulus in the x_1x_3 plane.

elastic constants are visualized by a plot of the directional dependence of the Young modulus in the x_1x_3 plane. It can be seen that the Young modulus is the highest in the transversely isotropic plane ($E_1 = 38.66$ GPa) and the smallest in direction perpendicular to this plane ($E_3 = 1.55$ GPa). However, the Young moduli both in the in-plane and out-of-plane directions are incomparably smaller than those of graphite ($E_1 = 1.03$ TPa and $E_3 = 36.1$ GPa [18]), probably because of the porosity and the micromechanics of the GNPs in the studied material similar to the one suggested for GNPs embedded in a ceramic matrix in [10]. Nieto et al. [11] reported on the Young moduli of the bulk GNPs measured by nanoindentation with significantly different results ($E_3 = 8.7$ GPa and E_1 exhibiting a bi-modal distribution with the values $E_1 = 10.3$ GPa and $E_1 = 15.2$ GPa). This indicates that the elasticity of the GNP bulk material is strongly amplitude-dependent. The elastic moduli determined by the ultrasonic measurements (amplitudes $\varepsilon \approx 10^{-6}$) correspond to purely elastic straining of the GNPs, including reversible sliding of the platelets, while for much larger strains the material is subjected to under the indenter, the measured elasticity corresponds probably also to folding of the platelets, pore closing and irreversible sliding. As a result, the elasticity determined by nanoindentation is much less anisotropic, since the highly oriented spatial arrangement of the GNPs deteriorates under the large loads induced by the indenter.

The resulting set of elastic coefficients c_{ij} can be possibly also used for rough estimates of the anisotropic elasticity of the CMC including some given amount GNPs by means of some rule of mixtures. For example, for the silicon nitride/GNP composite reported in [10], the Hill averaging method (using E =324 GPa for pure silicon nitride and the above obtained results $E_1 = 38.66$ GPa and $E_3 = 1.55$ GPa for GNPs) gives $E_1 = 273$ GPa and $E_3 = 168$ GPa. However, the experimental results $E_1 = 308$ GPa and $E_3 = 240$ GPa for this CMC [10] are significantly higher. This difference may indicate either that the GNPs embedded in ceramic matrices are better anchored than those in the examined material, or that the elasticity of the bulk GNPs is still significantly softened by porosity and weak interconnections between the individual platelets.

5. Conclusions

The ultrasonic measurements reported in this paper show that the bulk GNP material under study is highly anisotropic in acoustic properties such as speed of ultrasonic longitudinal and transverse waves and their attenuation.

The corresponding elastic coefficients are significantly more anisotropic than those obtained previously by nanoindentation, but simultaneously much less anisotropic that the elastic constants of graphite.

From the attenuation measurements, it is obvious that the elastic waves propagation in this material is damped at least by two different mechanisms: viscous energy dissipation probably due to mutual sliding of the GNPs (cf. [10]) and scattering of the waves on the layered porous structure. The attenuation coefficients obtained especially for the wave propagation perpendicular to the GNPs are very high, which suggest the possible application of the bulk GNPs as acoustic shock absorbers or as components of materials for acoustic energy redirection or cloaking.

Acknowledgments

The work of M.K., H.S. and M.L. has been financially supported by Czech Science Foundation (AdMat research center, 14-36566G). A.A. and A.N. would like to acknowledge Dr. Ali Sayir, Program Manager of High Temperature Aerospace Materials at the Air Force Office of Scientific Research and FA9550-12-1-0263 grant.

References

[1] C. Lee, X. Wei, J.W. Kysar, J. Hone, *Science* **321**, 385 (2008).

[2] K.H. Michel, B. Verberck, *Phys. Status Solidi B* **245**, 2177 (2008).

[3] A. Nieto, D. Lahiri, A. Agarwal, *Mater. Sci. Eng. A* **582**, 338 (2013).

[4] L.S. Walker, V.R. Marotto, M.A. Rafiee, N. Koratkar, E.L. Corral, *ACS Nano* **5**, 3182 (2011).

[5] O. Malek, J. González-Julián, J. Vleugels, W. Vanderauwera, B. Lauwers, M. Belmonte, *Mater. Today* **14**, 496 (2011).

[6] C. Ramirez, L. Garzón, P. Miranzo, M.I. Osendi, C. Ocal, *Carbon* **49**, 3873 (2011).

[7] G.D. Zhan, J.D. Kuntz, H. Wang, C.M. Wang, A.K. Mukherjee, *Philos. Mag. Lett.* **84**, 419 (2004).

[8] C. Ramírez, S.M. Vega-Diaz, A. Morelos-Gómez, F.M. Figueiredo, M. Terrones, M.I. Osendi, M. Belmonte, P. Miranzo, *Carbon* **57**, 425 (2013).

[9] P. Miranzo, E. García, C. Ramírez, J. González-Julián, M. Belmonte, M.I. Osendi, *J. Eur. Ceram. Soc.* **32**, 1847 (2012).

[10] H. Seiner, P. Sedlák, M. Koller, M. Landa, C. Ramírez, M.I. Osendi, M. Belmonte, *Compos. Sci. Technol.* **75**, 93 (2013).

[11] A. Nieto, D. Lahiri, A. Agarwal, *Carbon* **50**, 4068 (2012).

[12] M. Levy, H.E. Bass, R.R. Stern, *Handbook of Elastic Properties of Solids, Liquids, and Gases*, Vol. 1, *Dynamic Methods for Measuring the Elastic Properties of Solids*, Academic Press, New York 2000.

[13] R.G. Leisure, F.A. Willis, *J. Phys. Condens. Matter* **9**, 6001 (1997).

[14] P. Sedlák, H. Seiner, J. Zídek, M. Janovská, M. Landa, *Exp. Mech.* **54**, 1073 (2014).

[15] M. Landa, P. Sedlák, H. Seiner, L. Heller, L. Bicanová, P. Šittner, V. Novák, *Appl. Phys. A* **96**, 557 (2009).

[16] R. Truell, C. Elbaum, B.B. Chick, *Ultrasonic Methods in Solid State Physics*, Academic Press, New York 1969.

[17] M. Janovská, P. Sedlák, H. Seiner, M. Landa, P. Marton, P. Ondrejkovič, J. Hlinka, *J. Phys. Condens. Matter* **24**, 385404 (2012).

[18] E.J. Seldin, C.W. Nezbeda, *J. Appl. Phys.* **41**, 3389 (1970).